Research Article

A facile synthesis and controlled growth of various MoO_3 nanostructures and their gas-sensing properties

Shixiu Cao[1] · Cong Zhao[1] · Jing Xu[1]

Abstract
In this paper, three MoO_3 nanostructures were successfully synthesized via a hydrothermal method with the assistance of surfactants. We systematically explained the evolution process and proposed the possible formation mechanisms of the morphologies. The additives played an important role in the formation of MoO_3 morphologies. The gas sensing performance of the MoO_3 nanostructures to ethanol was also investigated. 3D porous nest-like MoO_3 nanostructures assembled with numerous nanorods exhibited excellent property. The results may be of great benefit to further investigations of synthesizing different MoO_3 nanostructures and their gas sensing applications.

Keywords MoO_3 · Nanostructures · Hydrothermal · Crystal growth · Sensors

1 Introduction

As a typical layered materials and n-type metal oxide semiconductors, MoO_3 nanomaterials have drawn considerable attention because of their superior physical and chemical properties [1, 2]. In recent years, they have been applied extensively as photochromic and electrochromic devices, gas sensors and catalysis, chemical and biological sensors, catalysts, energy storage, battery electrodes and supercapacitors [3–12]. The structures and morphologies of MoO_3 affect greatly its superior properties. Up to now, significant efforts have been devoted to constructing and controlling all kinds of nanostructures, such as nanoparticles, nanorods, nanowires, nanobelts, nanofires, and urchin-like nanostructures [13–18]. Notably, the porous nanostructures assembled with 1D or 2D nanocrystals, exhibited superior sensing properties in current studies [19]. Therefore, it is very important to develop a facile, shape and size-controlled route for the formation of the porous MoO_3 nanomaterials or architectures assembled from 1D nanocrystals.

In this paper, we synthesized three MoO_3 nanomaterials via a CTAB-assisted hydrothermal process, and reported their gas sensing properties. Besides, a possible formation mechanism was discussed in detail.

2 Experimental

2.1 Synthesis of samples

All chemical reagents were of analytic purity and applied directly without further purification. Firstly, sodium molybdenum ($Na_2MoO_4{\cdot}2H_2O$, 0.08 mmol), 10 ml 2 mol/L hydrochloric acid (HCl) solution, and cetyltrimethyl ammonium bromide (CTAB, 0.219 g, 0.365 g), were mixed in the 30 ml deionized water. Secondly, the pH value of the mixture was adjusted to 1–3.5 by dropping 2 mol/L hydrochloric acid (HCl). Thirdly, the final solution was transferred into a 100 ml Teflon-lined stainless autoclave. Then, the autoclave was maintained at 180–190 °C for 24 h, and cooled to room temperature naturally. Finally, the as-prepared samples were collected, and washed several times with

✉ Shixiu Cao, c28276152@126.com | [1]Research Institute for New Material Technology, Chongqing University of Arts and Science, Chongqing 402160, China.

SN Applied Sciences (2019) 1:1139 | https://doi.org/10.1007/s42452-019-0944-z

Received: 23 May 2019 / Accepted: 17 July 2019 / Published online: 3 September 2019

Table 1 Experimental condition of the four samples

Samples	$Na_2MoO_4{\cdot}2H_2O$ (mmol)	firstly added	Secondly added	Distilled water (ml)
I	0.08	HCl (10 ml)	CTAB (0.219 g)	30
II	0.08	CTAB (0.219 g)	HCl (10 ml)	30
III	0.08	CTAB (0.365 g)	HCl (10 ml)	30

distilled water and absolute ethanol, and dried finally in a vacuum oven at 80 °C for 10 h. To better describe the samples, when HCl is firstly added, as-prepared sample with CTAB (0.219 g) is named sample I. While HCl is posteriorly added, the powders obtained with the first addition of CTAB (0.219 g), CTAB (0.365 g), are named as sample II and sample III, respectively, as shown in Table 1.

2.2 Characterization of samples

The phase and crystallinity of the as-prepared samples were characterized via a powder X-ray diffraction (XRD) with a Rigaku D/Max-1200 diffractometry employing Cu Kα radiation operated at 30 kV and 100 mA. The size and morphology of as-obtained products were investigated using a Hitachi S-4300 scanning electron microscopy (SEM).

3 Results and discussion

3.1 XRD analysis

Figure 1 illustrates the diffraction pattern of three samples. All the peaks accord well with orthorhombic MoO_3 (α-MoO_3) of the JCPDS card (No. 05-0508), whatever the surfactants CTAB is firstly added or HCl is firstly added. The results show that addition order of the surfactants and HCl, does not affect the structure and purity of the synthesized samples. No diffraction peaks of any other impurities are observed, revealing the high purity of the prepared α-MoO_3. The strong and sharp peaks indicate that the products are highly crystallized.

3.2 SEM observation

Figure 2a shows the nanorods of the sample I. It can be seen that the size of the nanorods is about 100–200 nm in diameter and 1–3 μm in length (Fig. 2b). Figure 2c displays overall view in SEM image of the sample II, from which it could be observed that the MoO_3 products exhibit unique

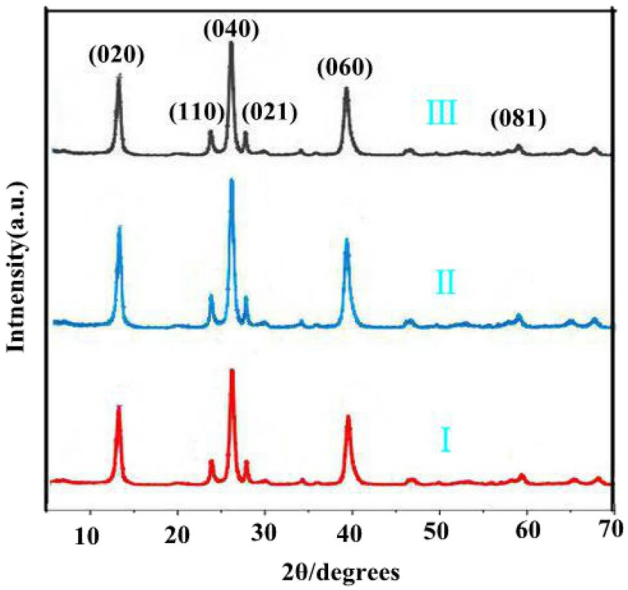

Fig. 1 XRD patterns of the products obtained

hierarchical nest-like architecture and these nest-like architectures with a diameter of about 3 μm link each other. Figure 2d shows that the magnified nest-like MoO_3 architectures are self-assembled by numerous nanorods, which have length of 300–500 nm and diameter of 50–100 nm. Figure 2e, f shows a SEM image of the MoO_3 nanosheets. The numerous nanosheets aggregate irregularly to flower-like architecture. And the size of the flower-like architecture is about 5 μm in diameter (Fig. 2e). As shown in Fig. 2f, the size of the nanosheets is about 500 nm–3 μm in width and 200 nm in thickness.

3.3 Growth mechanism

Theoretically, Na_2MoO_4 and HCl firstly reacted with each other to form H_2MoO_4. Then, under the hydrothermal conditions, the intermediate species (H_2MoO_4) decomposed and massive MoO_3 crystal nuclei were formed into nanocrystals [Eqs. (1)–(3)] [8]. In fact, due to the hydrothermal acidic system with high pressure, a part of MoO_3 crystal would dissolve into the H_2MoO_4. Large amount of small recrystallized MoO_3 might be formed immediately along with the large MoO_3 grain gradually dissolving in the solution. The crystal growth of MoO_3 was a delicate balance between the circulating dissolution and recrystallization process of MoO_3. The chemical reaction equations about the formation process of MoO_3 can be described as follows:

$$MoO_4^{2-} + H^+ \rightarrow HMoO_4^- \quad (1)$$

$$HMoO_4^- + H^+ \rightarrow H_2MoO_4(aq) \quad (2)$$

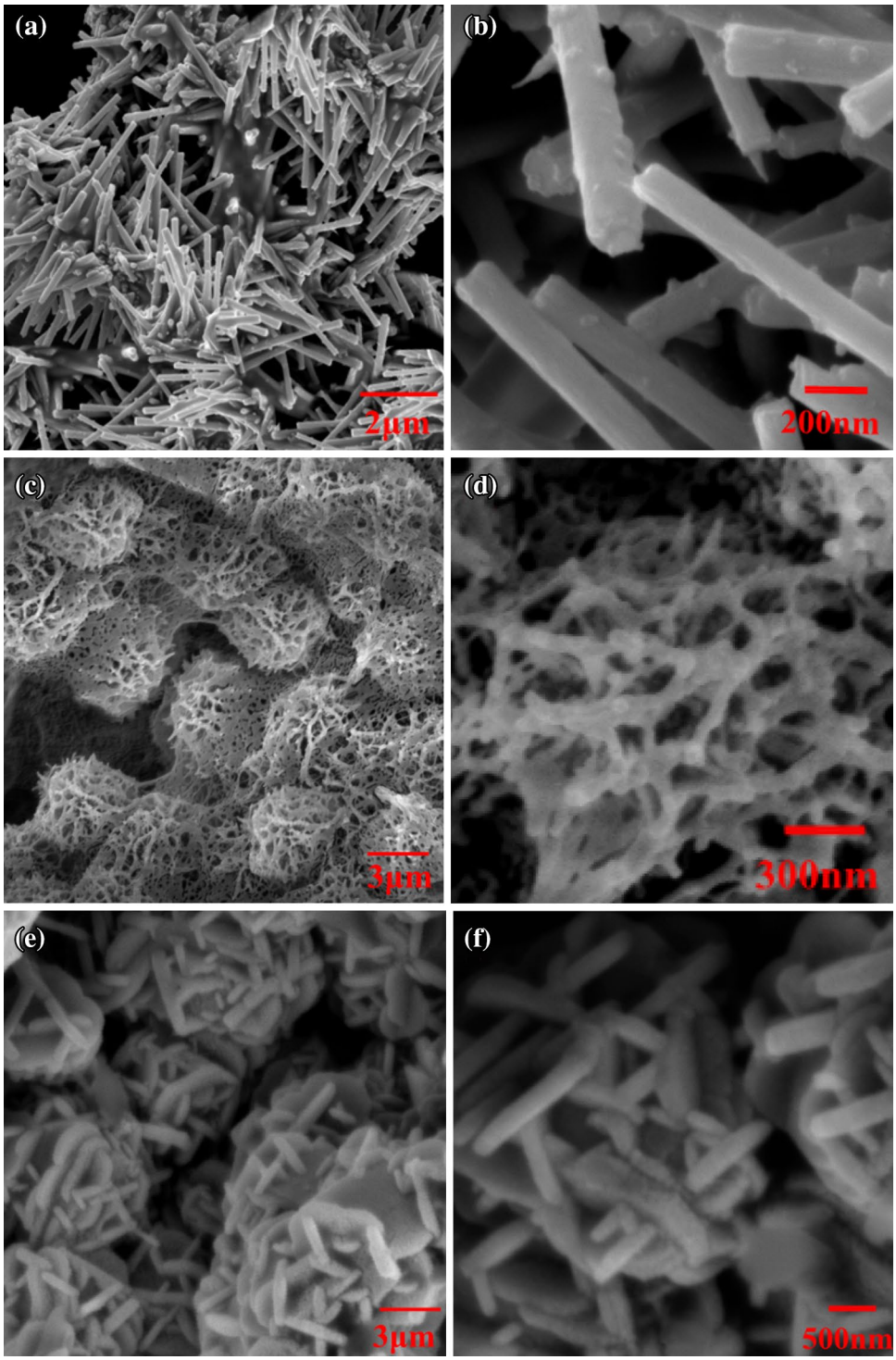

Fig. 2 SEM images of **a**, **b** sample I, **c**, **d** sample II and **e**, **f** sample III

$$H_2MoO_4(aq) \rightarrow MoO_3 \cdot H_2O \quad (3)$$

Figure 3 shows a possible growth mechanism of the three samples. As a positive ionic surfactant, CTAB ionizes completely in water. As shown in Fig. 3a, when HCl was firstly added, Na_2MoO_4 and HCl firstly reacted to form H_2MoO_4. And H_2MoO_4 decomposed and large amount of MoO_3 nanocrystals obtained. The later added CTAB played an important role in the formation of MoO_3 nanorods. The growth of orthorhombic α-MoO_3 with highly anisotropical structure, was influenced greatly by reaction conditions [20, 21]. It is reported that the interactions in α-MoO_3 between layers along [010] direction were weak van der Waals forces, but the interactions along [001] direction

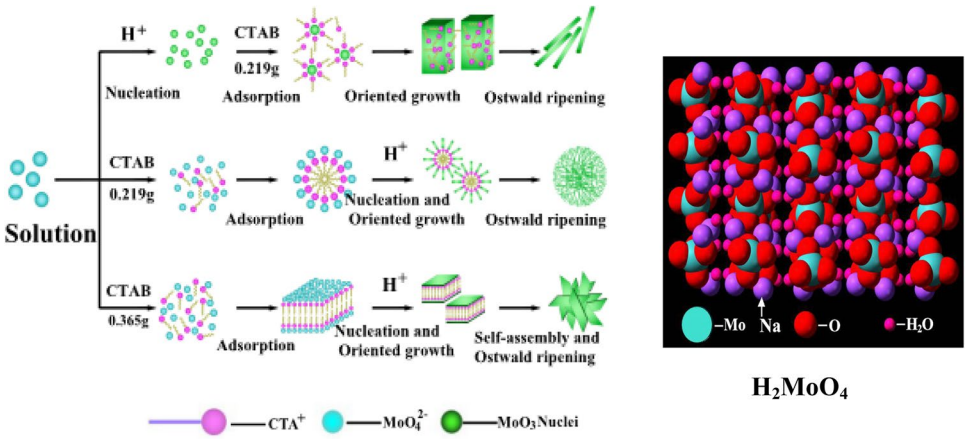

Fig. 3 Schematic illustration of the possible formation process for three MoO_3 nanostructures

were strong covalent bonds. In other words, more energy would be released if the α-MoO_3 nanocrystals grew along [001] direction. So, it is proposed that the later added CTAB tended to adsorb on ± (010) and ± (100) crystal surfaces of the α-MoO_3 nanocrystals, enhancing the growth rate along the [001] direction. Therefore, later added CTAB acted as an essential structure-directing agent in the formation of α-MoO_3 nanorods, along with the hydrothermal reaction proceeding.

When the concentration of CTAB reached the critical micelle concentration (CMC) [14, 22], CTAB micelles appeared. As shown in Fig. 3b, in the spherical micelles, the lipophilic groups tended to move inward and hydrophilic groups outward. However, the MoO_4^{2-} anions would combine with the CTA^+ cations to form the CTA^+–MoO_4^{2-} ions pairs due to the electrostatic interactions. When the HCl was later added, the strong interactions between H^+ and MoO_4^{2-} would suppress the attraction of MoO_4^{2-} by CTA^+. So, H_2MoO_4 decomposed and large amount of MoO_3 crystal nuclei, adsorption on the spherical micelles, were formed. According to the above analysis, we could can draw a conclusion that, in the acidic environment, the α-MoO_3 nanocrystals adsorption on the spherical micelles would grow to nanorods along the preferred orientation of [001] direction. As a result, the 3D nest-like α-MoO_3 nanostructures assembled with numerous nanorods were formed.

According to previous literatures, the different morphologies CTAB micelles appeared, along with the difference of the CTAB concentration and reaction temperature. As shown in Fig. 3c, 0.365 g CTAB was firstly added, CTAB laminar micelles appeared. The MoO_4^{2-} anions tended to gather between two layers due to the interaction force of the CTA^+–MoO_4^{2-} ions pairs. So, after HCl was added, α-MoO_3 nanocrystals were obtained between two layers and grew gradually into sheets. On the other hand, the nanosheets had two exposed surface and surface energy was high. Thus, in order to reduce the surface energy, the neighboring nanosheets were inclined to share an angle [23]. When the reaction time was long enough, nanocrystals grew into nanosheets and the flower-like α-MoO_3 nanostructures were obtained.

3.4 Gas-sensing properties

Figure 4a showed the gas sensing properties of the MoO_3 nanostructures fabricated sensors to ethanol at operating temperature from 200 to 450 °C. The optimum working temperature is 350 °C. The gas response increased with the temperature increasing when the temperature is below 350 °C. While the temperature exceeded 350 °C, the gas response decreased along with temperature increasing. The highest gas responses for the samples (I, II, III) to ethanol were estimated to be 35, 45, 39, respectively.

Figure 4b showed the response of the samples to ethanol under the different concentrations. Along with the increasing of concentrations, the gas responses all have a remarkable increase. Moreover, the nest-like α-MoO_3 structures exhibited more excellent performance. It may be just because that the nanoporous nest-like hierarchical nanostructures had the sufficient nano/micro reaction rooms for chemical reaction and effective diffusion channels for gases.

4 Conclusions

In summary, different morphologies of MoO_3 were successfully prepared via a simple CTAB-assisted hydrothermal process. As an assembling and structure directing agent to controllable, CTAB played a critical role in producing MoO_3 morphologies. The nanorod-assembled nest-like α-MoO_3 hierarchical structures exhibited superior gas sensing performance to ethanol. The results represent an advance of the porous hierarchical nanostructures in further enhancing the functionality of gas

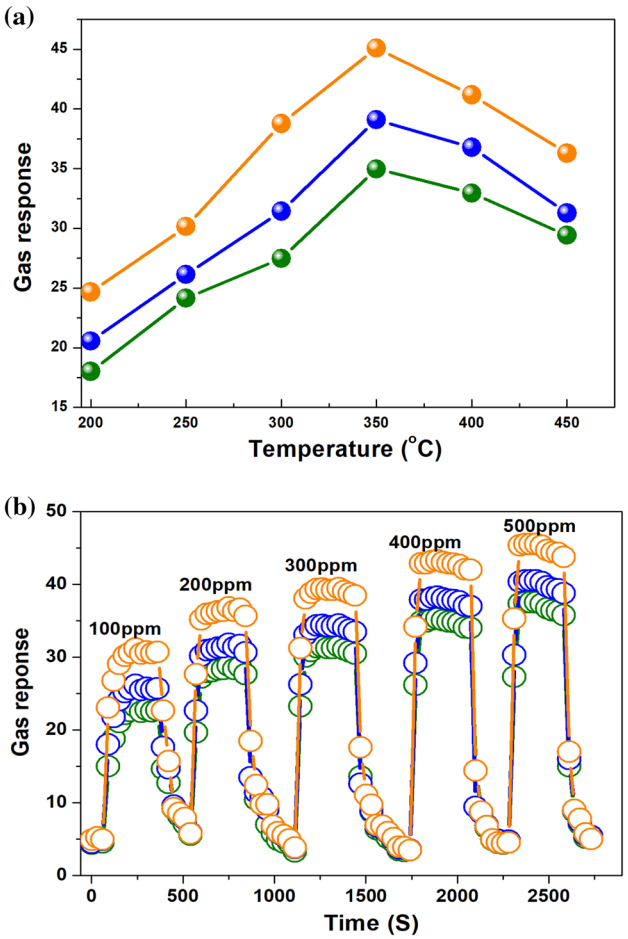

Fig. 4 Temperature versus gas response of the sensors made of MoO_3 to 400 ppm (**a**); Ethanol concentration versus gas response at 350 °C (**b**). Green line, blue, orange line for sample I, III, II, respectively

sensors. Moreover, this facile method may be extended to the synthesis of other oxides.

Acknowledgements The authors acknowledge the financial support to this work from the open project of Key Lab of Advanced Materials of Yunnan Province (2016cx06), the Basic and Frontier Research Program of Chongqing Municipality (cstc2016jcyjA0567, cstc2017jcyjBX0051), the Science and Technology Research Program of Chongqing Education Commission (KJ1711282, KJ1711283).

Compliance with ethical standards

Conflict of interest The authors declare that they have no conflict of interest.

Ethical approval This article does not contain any studies with human participants or animals performed by any of the authors.

References

1. Zeng W, Zhang H, Li YQ, Chen WG (2014) Net-like MoO_3 porous architectures: synthesis and their sensing properties. J Mater Sci Mater Electron 25:338–342
2. Li XB, Ma SY, Li FM, Chen Y, Zhang QQ, Yang XH et al (2013) Porous spheres-like ZnO nanostructure as sensitive gas sensors for acetone detection. Mater Lett 100:119–123
3. Xue HT, Yang X, Guan ZQ, Cheng YH, Tsang SW, Lee CS (2015) Low temperature sonochemical synthesis of morphology variable MoO3 nanostructures for performance enhanced lithium ion battery applications. Electrochim Acta 185:83–89
4. Han B, Lee KH, Lee YW, Kim SJ, Park HC, Hwang BM et al (2015) MoO_3 nanostructured electrodes prepared via hydrothermal process for lithium ion batteries. Int J Electrochem Sci 10:4232–4240
5. Yogananda HS, Nagabhushana H, Naik R, Prashantha SC (2017) Calcination temperature dependent structural modifications, tailored morphology and luminescence properties of MoO_3 nanostructures prepared by sonochemical method. J Sci Adv Mater Dev 1–9
6. Wang LN, Zhang X, Ma Y, Yang M, Qi YX (2016) Rapid microwave-assisted hydrothermal synthesis of one-dimensional MoO_3 nanobelts. Mater Lett 164:623–626
7. Liu YL, Yang S, Lu Y, Podval'naya NV, Chen W, Zakharova GS (2015) Hydrothermal synthesis of *h*-MoO_3 microrods and their gas sensing properties to ethanol. Appl Surf Sci 359(2015):114–119
8. Yang YL, Shen Y, Li Z (2015) Reaction time effect of straw-like MoO_3 prepared with a facile, additive-free hydrothermal process. RSC Adv 5:255–260
9. Castro IAD, Datta RS, Ou JZ, Gomez AC, Sriram S, Daeneke T, Zadeh KK (2017) Molybdenum oxides from fundamentals to functionality. Adv Mater 29:1701619
10. Alsaif MMYA, Chrimes AF, Daeneke T, Balendhran S, Bellisario DO, Son Y et al (2016) High-performance field effect transistors using electronic inks of 2D molybdenum oxide nanoflakes. Adv Funct Mater 26:91–100
11. Zhang BY, Zavabeti A, Chrimes AF, Haque F, O'Dell LA, Khan H et al (2018) Degenerately hydrogen doped molybdenum oxide nanodisks for ultrasensitive plasmonic biosensing. Adv Funct Mater 28:1706006
12. Alsaif MMYA, Latham K, Field MR, Yao DD, Medehkar NV, Beane GA et al (2014) Tunable plasmon resonances in two-dimensional molybdenum oxide nanoflakes. Adv Mater 26:3931–3937
13. Xia YC, Wu CS, Zhao NY, Zhang H (2016) Spongy MoO_3 hierarchical nanostructures for excellent performance ethanol sensor. Mater Lett 171:117–120
14. Li YQ, Liu TM, Li TM, Peng XH (2015) Hydrothermal fabrication of controlled morphologies of MoO_3 with CTAB: structure and growth. Mater Lett 140:48–50
15. Yang S, Liu YL, Chen W, Jin W, Zhou J, Zhang H, Zakharova GS (2016) High sensitivity and good selectivity of ultralong MoO_3 nanobelts for trimethylamine gas. Sensor Actuat B-Chem 226:478–485
16. Li TM, Zeng W, Zhang YY, Hussain S (2015) Nanobelt-assembled nest-like MoO_3 hierarchical structure: hydrothermal synthesis and gas-sensing properties. Mater Lett 160:476–479
17. Alizadeh S, Hassanzadeh-Tabrizi SA (2015) MoO_3 fibers and belts: molten salt synthesis, characterization and optical properties. Ceram Int 41:10839–10843
18. Phuruangrat A, Cheed-Im U, Thongtem T, Thongtem S (2016) High visible light photocatalytic activity of Eu-doped MoO_3

nanobelts synthesized by hydrothermal method. Mater Lett 172:166–170
19. Phuruangrat A, Ham DJ, Thongtem S, Lee JS (2009) Electrochemical hydrogen evolution over MoO_3 nanowires produced by microwave-assisted hydrothermal reaction. Electrochem Commun 11:1740–1743
20. Li XL, Liu JF, Li YD (2002) Low-temperature synthesis of large-scale single-crystal molybdenum trioxide (MoO_3) nanobelts. Appl Phys Lett 81:4832–4834
21. Lou XW, Zeng HC (2002) Hydrothermal synthesis of α-MoO_3 nanorods via acidification of ammonium heptamolybdate tetrahydrate. Chem Mater 14:4781
22. Sinaim H, Ham DJ, Lee JS, Phuruangrat A, Thongtem S, Thongtem T (2012) Free-polymer controlling morphology of α-MoO_3 nanobelts by a facile hydrothermal synthesis, their electrochemistry for hydrogen evolution reactions and optical properties. J Alloys Compd 156:172–178
23. Wang J, Zeng W, Wang ZC (2016) Assembly of 2D nanosheets into 3D flower-like NiO: synthesis and the influence of petal thickness on gas-sensing properties. Ceram Int 42:4567–4573